A Theoretical and Experimental Examination of Thermal Ink Jet Nucleation Criteria

Robert Cornell
Lexmark International Inc., Lexington, Kentucky

Abstract

A typical ink jet heater is exposed to a power density on the order of 10^9 W/m^2. The resulting temperature transient in the thin film structure exceeds 10^8 K/s. After several microseconds nucleation occurs, and ink at the heater surface explodes into vapor. The liquid in the firing chamber is near atmospheric pressure so nucleation occurs at the super heat limit, not the critical point. The superheat limit can be determined from the equation of state and the mechanical stability criterion. Another method applies molecular kinetics to determine the superheat limit. Both methods result in a band of uncertainty around the actual nucleation temperature. Since this temperature determines initial bubble pressure, and ultimately, bubble size and droplet size, a new technique is required. To that end, this paper presents a bubble reliability function. Integration of the nucleation rate equation, combined with reliability statistics and transient heat transfer, predicts nucleation behavior over a wide range of power densities. Laboratory data is also presented to verify the model accuracy.

Nucleation Models

It has been well established that thermal ink jet operates in the film boiling regime.[1] This is in contrast to the more general multiphase flow applications which operate below the critical heat flux point on the boiling curve. The film boiling regime is aptly referred to as burnout. In general industrial applications, this regime isn't usually the intended result. Sometimes it's the end product of an accident.[2][3]

A significant difference between ink jet and the more traditional boiling heat transfer applications is the amount of superheat required to nucleate a bubble. While the traditional applications spend time and money to groove heat transfer surfaces to achieve cavity initiated boiling at low superheat, the thermal ink jet application requires defect free, smooth surfaces to delay nucleation until the highest possible superheat is reached. The advantage of high temperature superheat is crisp nucleation and a high pressure pulse to propel the droplet at speeds of 10^+ m/s.

Since nucleation from trapped gas in grooved cavities is not the boiling regime of thermal ink jet, it will not be examined in this paper.

Thermodynamic Limit of Superheat

Classical thermodynamics[4] takes a macroscopic point of view, treating phase change as an equilibrium condition. Yet a microscopic viewpoint reveals that phase change cannot occur under equilibrium conditions. Phase change requires mass and heat flux at the vapor-liquid interface. Heat flux requires a temperature gradient. The existence of a temperature gradient implies non-equilibrium conditions. This is often referred to as the fundamental paradox.[5] In the following discussion of nucleation physics, the microscopic viewpoint is adopted.

Liquid may be superheated without a phase change occurring. Liquid that is superheated above the saturation condition is in a metastable state. For example, point A of Figure 1 is on the saturation curve. Yet the system may experience an isothermal increase in volume without phase change. The familiar criterion of mechanical stability is given by $(dP/dV)_T < 0$. Then the limit of the metastable region is where $(dP/dV)_T = 0$, shown as point B in Figure 1. The locus of these metastable limits, forms the spinodal curve.[6]
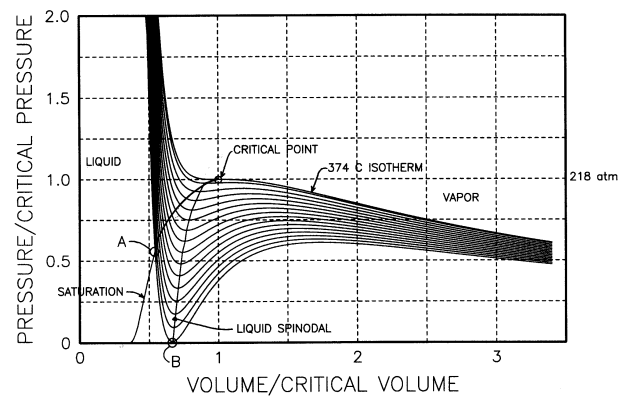

Figure 1. van der Waals Equation of State

Applying the mechanical stability criterion to the equation of state permits a prediction of the spinodal limit, or the thermodynamic limit of superheat. The isotherms plotted in Figure 1 are computed with van der Waals equation of corresponding states. The intersection of the liquid spinodal with the line corresponding to one atmosphere is on the isotherm that defines the superheat limit. Depending on which equation of state is used, this method predicts the superheat limit is between 0.84 to 0.92 of the critical temperature, for many fluids.

This method of computing superheat limit has some uncertainties, such as, which equation of state to use. The other uncertainty is this; the spinodal limit only predicts where the phase change is certain to occur. Yet there is a finite probability that phase change will occur somewhere between points A and B. The thermodynamic limit of superheat is unsuitable for use in thermal ink jet bubble dy-

namics models because the above mentioned uncertainties make nucleation temperature just an adjustable variable.

Kinetic Limit of Superheat

Before the fire pulse is turned on, ink in the bubble chamber is subcooled, saturated liquid in quasi-thermal equilibrium. With the application of i^2R power in the thin film resistor, the liquid at the chip surface heats rapidly. With the heat transfer comes increased molecular motion and local density fluctuations in the liquid. The density fluctuations will push into the metastable region discussed in the last section. When vapor embryos appear in the liquid, some will collapse and some will grow. The physics of this embryonic growth process is revealed by examining the molecular kinetics of the liquid vapor system. The details of this process are far too involved to review in this paper. Suffice it to say, it is possible to develop a function that computes the critical embryo radius (Reference 7 and 11). Furthermore, it is possible to determine the stability of the embryo. The loss of one molecule from a critically sized embryo will cause instantaneous collapse. In contrast, the addition of one molecule will cause the embryo to spontaneously grow. The rate by which embryos grow from n to $n + 1$ molecules is given by:[7]

$$J = 1.44 \times 10^{40} \left(\frac{\rho_L^2 \sigma}{M^3} \right)^{0.5} \exp\left[\frac{-1.213 \times 10^{24} \sigma^3}{T_L \left(\eta P_{sat} - P_L \right)^2} \right] \quad (1)$$

$$\eta = \frac{P_L + (2\sigma / R_E)}{P_{SAT}} = \exp\left[\frac{(P_L - P_{sat})M}{\rho_L N_A K_B T_L} \right]$$

J = *volumetric nucleation rate (l/m^3s)*

P_L = *liquid pressure (Pa)*

P_{SAT} = *saturated vapor pressure (Pa)*

T_L = *liquid temperature (K)*

ρ_L = *liquid density (kg/m^3)*

M = *molar weight of the liquid (kg/mol)*

K_B = *Boltzmann constant (J/K)*

N_A = *Avogadro number (molecules/mol)*

σ = *liquid surface tension (N/m)*

R_E = *critical embryo radius (m)*

In the above expression, P_{SAT} and σ are functions of liquid temperature T_L. The solution of equation (1) is shown in Figure 2. The function is plotted for water. Saturation pressure is computed by cubic Lagrangian interpolation of the steam tables. Similarly, surface tension is interpolated from tabular data.[8] There are regression equations for $\sigma_{H20}(T)$ in the literature,[9,10] but they generally have the largest error in the high temperature region—the region of interest for ink jet nucleation.

In this analysis, it is assumed that ink behaves like water. While ink is a mixture of humectants, colorants and other chemicals, water is the primary constituent, on a mole basis. For typical Lexmark inks, the mole fraction of water is greater than 90%. With this in mind, the assumption that water and ink should have similar molecular kinetics is rea-

sonable. Also, this analysis assumes that nucleation is homogeneous. It has been shown[11] that the homogeneous mode dominates over the heterogeneous mode for solid-liquid-vapor contact angles less than 68°. In thermal ink jet applications, the contact angle is generally less than this.

Band of Uncertainty

The ambiguity concerning the superheat limit of water is apparent in Figure 2. The thermodynamic limit of superheat depends on which equation of state is used, as shown on the bottom axis of the plot. The superheat limit, as defined by kinetic theory, depends on what level of (J) is selected as the threshold. The right hand plot axis shows the variety of (J) values cited in reference 11.
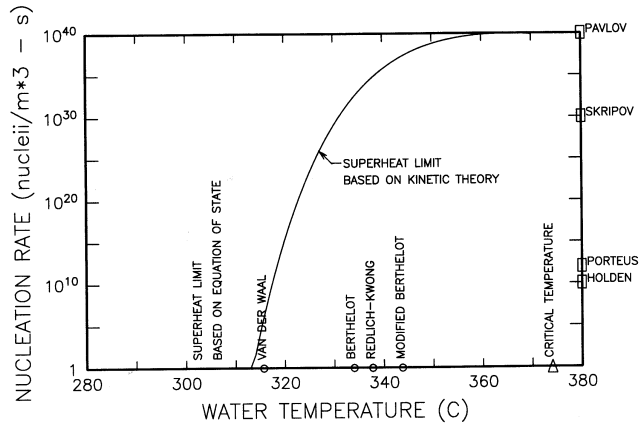

Figure 2. Nucleation Rate of Water

Figure 2 indicates a band of uncertainty from about 314 to 360 °C. Over this temperature range, saturated steam pressure varies from 10.4 to 18.7 MPa. Since the pressure impulse associated with nucleation is the driving means for thermal ink jet, this much pressure variation makes even kinetic theory an unsuitable predictor for accurate bubble growth models. However, merging kinetic theory with reliability statistics provides a solution to this dilemma.

Bubble Reliability

In addition to a steep temperature gradient into the ink, the heater surface is not isothermal. The edges are much cooler than the center. Also, the temperature field is highly transient during the fire pulse. Given these conditions, it is illogical to pick a fixed temperature (T_l) or rate (J) to determine when nucleation occurs under the driving conditions imposed by thermal ink jet devices.

The bubble dynamics model developed at Lexmark uses the following approach. The nucleation rate equation is integrated over time and space. Then reliability statistics are applied after each time increment to determine when nucleation probability goes to unity. The bubble reliability function is derived below. In this derivation, an active molecule is defined as having sufficient kinetic energy to result in vapor embryo growth. While an inactive molecule is below this threshold.

N_S = *number of active molecules*

N_F = *number of inactive molecules*

$N = N_S + N_F$ = *total molecules*   (2)

t = *time*

$P(t) = N_F(t)/N$ = *probability of failure* (*no bubble*)   (3)

$R(t) = N_S(t)/N = 1 - P(t)$ = *bubble reliability*   (4)

The rate of change of the probability is:

$$\frac{\Delta P}{\Delta t} = \frac{N_F(t + \Delta t) - N_F(t)}{N/\Delta t}$$

The instantaneous rate of change is:

$$\frac{dP}{dt} = \lim_{\Delta t \to 0} \frac{\Delta P}{\Delta t} = \frac{1}{N}\frac{dN_F(t)}{dt} \qquad (5)$$

Let $\lambda(t)$ equal the rate at which inactive molecules become active molecules during each time interval:

$$\lambda(t \to t + \Delta t) = \left(\frac{N_F \text{ reduction during time interval}}{N_F \text{ at beginning of time interval}}\right)/\Delta t$$

$$\lambda(t \to t + \Delta t) = \frac{N_F(t) - N_F(t + \Delta t)}{N_F(t)/\Delta t} \qquad (6)$$

$$\lambda(t) = \lim_{\Delta t \to 0}(t \to t + \Delta t) = \frac{-1}{N_F(t)}\frac{dN_F(t)}{dt}$$

Substitution of (3) and (5) into (6) yields:

$$\lambda(t) = \frac{-1}{P(t)}\frac{dP(t)}{dt} \qquad (7)$$

Integrating (7) over the fire pulse (tp) with initial conditions:

$$N_F(0) = N \text{ therefore } P(0) = 1$$

$$\int_0^{tp} \lambda dt = \int_1^{P(t)} \frac{-1}{P(t)}dt = -1nP(t) \qquad (8)$$

$$P(t) = \exp\left[-\int_0^{tp} \lambda(t)dt\right]$$

Then bubble reliability is:

$$R(t) = 1 - P(t) = 1 - \exp[-\int_0^{tp}\lambda(t)dt] \qquad (9)$$

The form of equation (9) is similar to the distribution free, general equation relating hardware reliability to failure rate,[12] except in this case, $\lambda(t)$ refers to a nucleation rate not the hazard function. In a typical reliability problem, $\lambda(t)$ is derived from hardware test data. For bubble reliability, the expression for $\lambda(t)$ comes from the integration of equation (1) over space and time.

$$\lambda(t) = \oint J[T_L(x, y, z, t)]dV \qquad (10)$$

The transient temperature field is computed by the 2D conduction equation.

$$\frac{\partial}{\partial x}\left(K_x\frac{\partial T}{\partial x}\right) + \frac{\partial}{\partial y}\left(K_y\frac{\partial T}{\partial y}\right) + Q = \rho C_p\frac{\partial T}{\partial t} \qquad (11)$$

Equations (9) and (10) are similar in form to those presented by Asai.[13]

Simulation Results

An application specific-finite element model[14] was created in *APL* to mesh the domain and solve equation (11). Because the fire pulse is only a few microseconds long, the domain can be limited to a small region in the vicinity of the heater. Far field effects may be ignored on this time scale. Typical results for a high power density pulse are shown in Figure 3. The steep gradients are apparent. Figure 4 shows the temperature field for a low power density pulse, i.e. the same structure, with the same electrical energy, but lower current delivered over a much longer time. Low power density results in lower surface temperatures due to lateral diffusion into the aluminum electrode region and the silicon substrate.
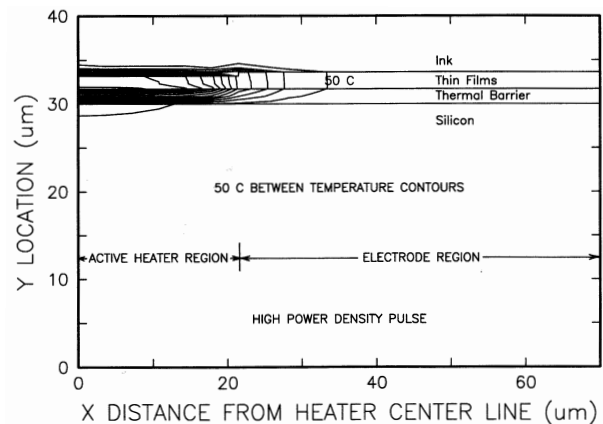

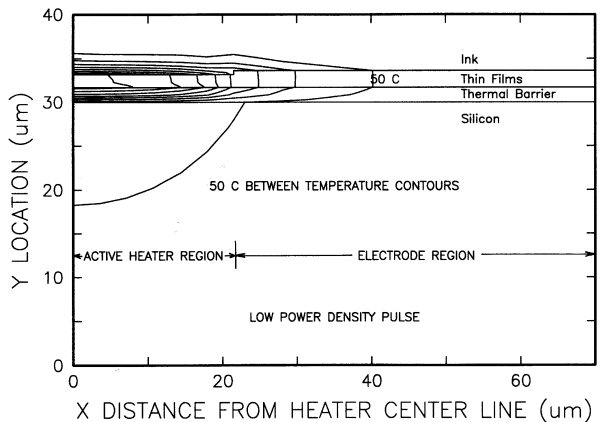*Figure 3. High Power Density Temperature Field*

Figure 4. Low Power Density Temperature Field

The solution of equation (9) is shown in Figure 5 for the high power density pulse. This surface plot provides a snapshot of nucleation probability during the fire pulse. Ide-

ally, ink over the entire heater surface nucleates simultaneously. However due to thermal diffusion into the aluminum wiring, ink near the heater edge takes longer to reach temperatures high enough for nucleation. In fact, the entire heater never participates in the nucleation process, making the effective heater size smaller than the geometric heater size.[15] This can be seen in the contour lines of Figures 3 and 4. Low power density fire pulses aggravate this situation, as shown in Figure 6.
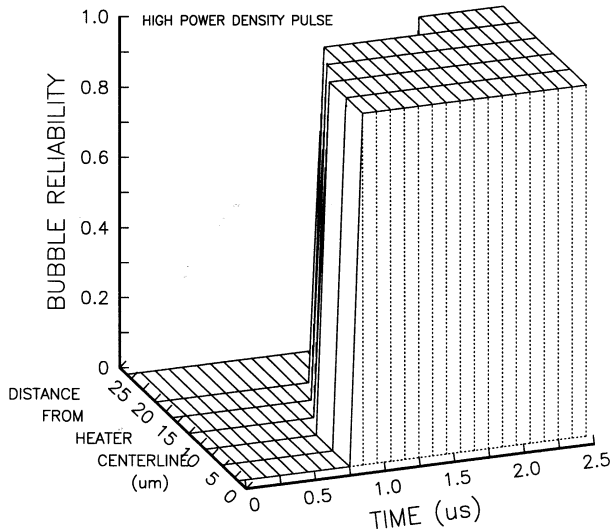
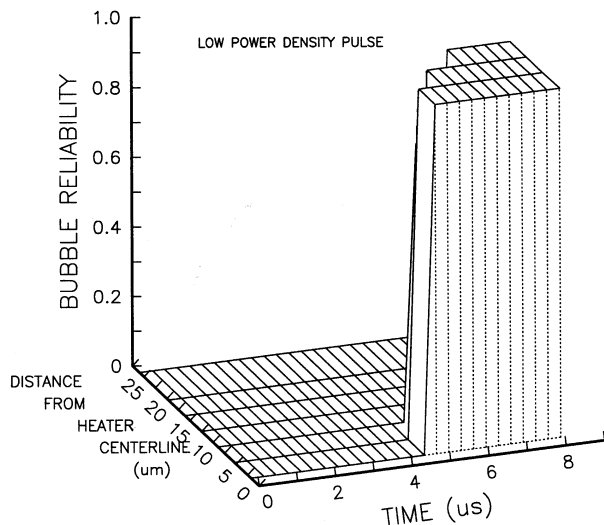

Figure 5. High Power Density Bubble Reliability

Figure 6. Low Power Density Bubble Reliability

Experimental Results

In situ measurements of nucleation temperature in a working ink jet device have yet to be made at Lexmark. The gradients and transients involved make this a difficult experiment to run. However, indirect means have been used to verify the bubble reliability model.

The first method used to verify the model was an open pool bubble watcher. The heater chip was covered with a thin layer of deionized water. Then a cover slide was used

to flatten out the liquid. The heater was pulsed at a very low rate (100 Hz) to minimize bulk heating effects. Bubble dynamics were viewed at high magnification (400X) using a time delayed Xenon strobe. Heater power density was measured with a Tektronix DSA602A digital storage oscilloscope. A photoelectric detector was used to measure the strobe intensity with respect to the fire pulse. These timing measurements indicated the best possible resolution was about 1 µs using this technique, not quite good enough.

An alternative technique was developed to perform experimental verification of the bubble reliability model. The alternative technique used the fire pulse as a nucleation clock. The fire pulse width was controlled to 0.1 µs resolution. The improved technique still used a strobe, but the strobe timing was less critical. For a given power density, the width of the fire pulse was adjusted until the heater just showed nucleation activity. This minimum pulse width corresponded with the onset of bubble nucleation.

Using this technique to view the bubble, it was possible to measure time to nucleation with 0.1 µs resolution at varying power densities. This was repeated using several formulations of yellow ink and several dyeless ink formulations.

Discussion

The experimental and simulation results are shown together in Figure 7. The simulations are quite close to the measured results. The correlation between lab data and simulation results is further evidence that ink behaves like water, provided the mole fraction of water is sufficiently large.

A second set of data is also shown in Figure 7. In this case the fluid under study is isopropyl alcohol. For this fluid, P_{SAT} is computed using the Clausius-Clapeyron equation, and surface tension is estimated by.[16]

$$\sigma_{IPA} = 0.001 \times (22.9 - 0.0789T_L) \ (N/m) \qquad (12)$$

Figure 7 shows that water, isopropyl alcohol and various inks, have good correlation between experimental data and bubble reliability simulations over a wide range of power densities—an indirect yet compelling verification of the model.
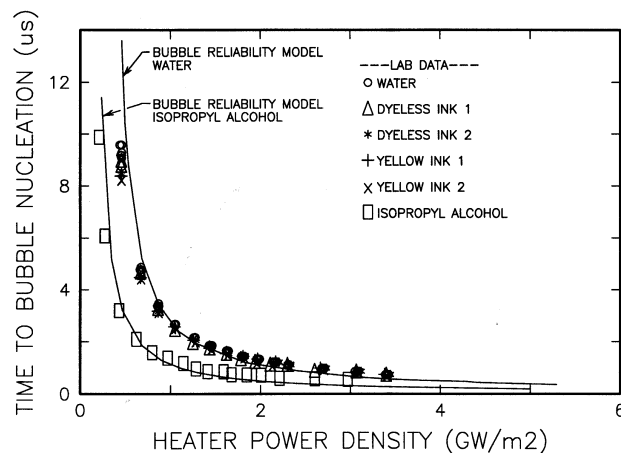

Figure 7. Lab Data and Bubble Reliability Results

Runge's Empirical Criteria

In 1992 an empirical criterion for ink jet nucleation was published by Runge.[17] It was the result of measuring nucleation times in an open pool bubble watcher with a strobe. Then the conduction equation was used to compute the temperature field corresponding to the observed nucleation time. Regression analysis led to the empiric expression is shown below.

$$K = \frac{T_{wall}}{230 + 0.16(\partial T / \partial y)}$$

$\dfrac{\partial T}{\partial y} = gradient\ at\ ink - heater\ interface\ (C/\mu m)$

$Twall = temperature\ at\ the\ ink\text{-}heater\ interface\ (C)$

$K < 1\ no\ nucleation$

$K = 1\ nucleation$

$K > 1\ not\ allowed$

$$(13)$$

At high power densities, i.e., high heat fluxes, this equation predicts nucleation temperatures greater than the critical point. Since nature does not allow this, *K* greater than unity is not allowed in the above expression. But print heads may be driven at high power densities. How is this possible? This discrepancy can be explained with the bubble reliability model.

The 2D conduction equation (11) was solved over a wide range of power densities for a standard thin film structure. Then knowing the time-temperature field, nucleation probability was computed by equation (9) and by equation (13). Nucleation times computed by both methods were similar, but not equivalent (Figure 8). At high power densities, equation (13) predicted nucleation times a few tenths of a microsecond later than the bubble reliability method. It is important to note, at high power densities the surface temperature is climbing at a rate of several hundred million degrees Kelvin per second. Under these driving conditions, a few tenths of a microsecond error in observed nucleation timing would incorrectly lead to a conclusion that the critical point was being exceeded. Figure 9 shows the surface temperatures corresponding to the nucleation times of the previous plot. The bubble reliability method never predicted nucleation temperatures greater than the critical point. Over the power density range shown, the nucleation temperature ranged from 329.7 to 331.7 °C.

Bubble Reliability and Bubble Growth

On the basis of the results shown in Figure 7, the bubble reliability model appears to be an effective means of predicting the onset of nucleation in a thermal ink jet device. Taking this the next step, the bubble reliability model was merged with the application specific-bubble growth model,[18] also written in *APL*. The merged models have proven to be accurate predictors of droplet size over a wide range of bubble chamber geometries, ink viscosities, bulk chip temperatures and pulsing conditions. Figure 10 shows a strong correlation between predicted droplet size and measured droplet size.
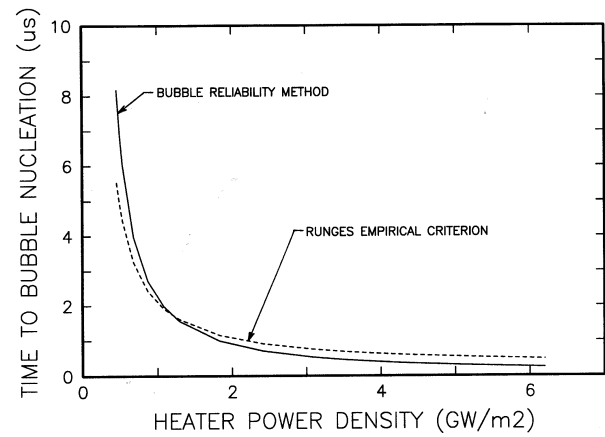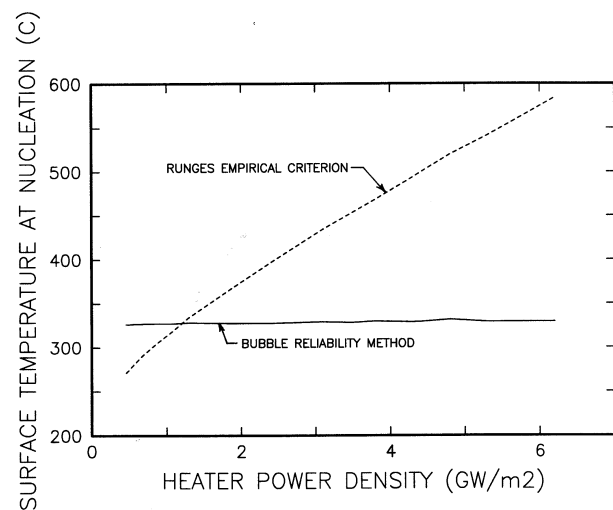

Figure 8. Nucleation Time Comparison

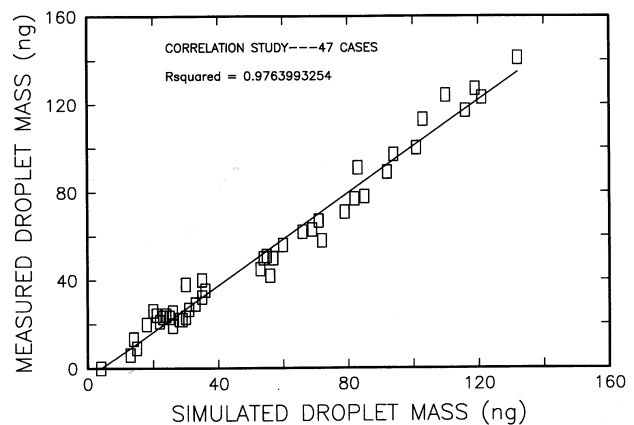*Figure 9. Nucleation Temperature Comparison*

Figure 10. Lab Data and Bubble Simulation Results

Conclusion

A bubble reliability model is derived. When applied to the nucleation rate equation, it predicts nucleation times over a

wide range of power densities. It also predicts the probability of nucleation as a function of time and heater position. Even under the highest heat flux conditions, the critical point is never exceeded. The model works well for water and a variety of water based inks. It also works well for isopropyl alcohol.

  Further experimental work is necessary to observe embryo formation on a nanosecond time scale.

References

1. A. Asai, S. Hirasawa and I. Endo, "Bubble Generation Mechanism in the Ink Jet Recording Process". *J. Imaging Tech.* Vol. **14**, No. 5, (1988).

2. M. Song and P. Turinsky, "Analytic Predictions of Boiling Film Stability for Conditions Consistent With Light Water Reactor Degraded Core", *Nuc. Science and Engr.* Vol. **101** (1989).

3. A. Inoue and M. Aritomi, "An Analytical Model of Vapor Explosion of a High Temperature Metal Droplet With Water Induced Pressure Pulse", *Proc. 20th Nat. Heat Trans. Symp*. (1983).

4. G. Van Wylen and R. Sonntag, "Fundamentals of Classical Thermodynamics", John Wiley and Sons, New York, 1973.

5. O. Jones, "Homogeneous Equilibrium and Nonequilibrium Phase Change", *Modern Developments in Multiphase Flow*, Rensselaer Polytechnic Institute (1996).

6. E. Fermi, *Thermodynamics*, Dover Publications, New York, 1956.

7. V. Carey, *Liquid-Vapor Phase Change Phenomena*, Hemisphere, Washington, 1992.

8. F. Kreith and M. Bohn, "Principles of Heat Transfer", 4th ed., Harper & Row, New York, l986.

9. National Bureau of Standards, "Release of Surface Tension of Water Substance", *The Int. Assoc. for Prop. of Steam* (1976).

10. G. Somayajulu, "A Generalized Equation for Surface Tension From the Triple Point to the Critical Point", *Int. J. of Thermophys.*, Vol. **9**, No. 4 (1988).

11. S. Van Stralen and R. Cole, "Boiling Phenomena" Hemisphere, Washington, 1979.

12. P. Tobias and D. Trindade, "Applied Reliability", Van Nostrand, New York, 1986.

13. A. Asai, "Application of Nucleation Theory to the Design of Bubble Jet Printers", *Japanese J. App. Phys*., Vol. **28**, No. 5, (1989).

14. L. Segerlind, "Applied Finite Element Analysis", John Wiley & Sons, New York, 1976.

15. R. Cornell, "A Theoretical and Experimental Examination of the Bubble Jet Energy Window", *Proc. IS&T 47th Annual Conf.* (1994).

16. J. Jasper, "The Surface Tension of Pure Liquid Compounds", *J Phys. Chem. Ref. Data.* Vol. **I**, (1972).

17. W. Runge, "Nucleation in Thermal Ink Jet Printers", *IS&T 8th Int. Cong. on Adv. in Non-Impact Printing Technologies,* (1992).

18. R. Cornell "Thermal Ink Jet - An Analysis of Heat Transfer and Bubble Growth Physics", *Lexmark Technical Note*, (1995).